NMR study of magnetic order, metamagnetic transitions, and low-temperature spin freezing in $Ca_3Co_2O_6$

G. Allodi* and R. De Renzi
Dipartimento di Fisica e Unità CNISM, Università degli Studi di Parma, Viale G. Usberti 7A, I-43100 Parma, Italy

S. Agrestini
Laboratoire CRISMAT, UMR 6508, Boulevard du Maréchal Juin, F-14050 Caen Cedex, France
Max Planck Institute for Chemical Physics of Solids, Nöthnitzerstr. 40, D-01187 Dresden, Germany

C. Mazzoli
European Synchrotron Radiation Facility, BP 220, 38043 Grenoble Cedex 9, France
Dipartimento di Fisica, Politecnico di Milano, Piazza Leonardo da Vinci 32, I-20133 Milano, Italy

M. R. Lees
Department of Physics, University of Warwick, Coventry CV4 7AL, United Kingdom
(Received 3 November 2010; published 14 March 2011)

We report on a ^{59}Co NMR investigation of the trigonal cobaltate $Ca_3Co_2O_6$ carried out on a single crystal, providing precise determinations of the electric field gradient and chemical shift tensors, and of the internal magnetic fields at the nonmagnetic Co I sites, unavailable from former studies on powders. The magnetic-field-induced ferri- and ferromagnetic phases at intermediate temperature (e.g., 10 K) are identified by distinct internal fields, well accounted for by purely dipolar interactions. The vanishing transferred hyperfine field at the Co I site indicates that the Co^{3+} (I) orbitals do not participate in the intrachain superexchange, in disagreement with a previous theoretical model. The strong Ising character of the system is confirmed experimentally by the field dependence of the resonance lines, indicating that local moments are saturated even at the phase boundaries. In the vicinity of the critical fields, nuclear spin-spin relaxations detect the spin-reversal dynamics of large magnetic assemblies, either Ising chain fragments or finite-size domains, which drive the metamagnetic transitions. Such collective excitations exhibit a glassy behavior, slowing down to subacoustic frequencies and freezing at low temperature. The relevance of such slow-fluctuation modes for the low-temperature multistep behavior reported in the magnetization is discussed.

DOI: 10.1103/PhysRevB.83.104408 PACS number(s): 75.30.Kz, 75.30.Et, 75.60.Jk, 76.60.−k

I. INTRODUCTION

The nature of magnetic order in the geometrically frustrated trigonal cobaltate $Ca_3Co_2O_6$, an Ising-type magnet exhibiting low-dimensional behavior, has been a puzzle for over a decade. The crystal structure of $Ca_3Co_2O_6$ (Fig. 1) may be viewed as the result of the alternate stacking along the c axis of face-sharing CoO_6 octahedra (Co I) and CoO_6 trigonal prisms (Co II) with a rather short Co I–Co II distance $c/4 = 2.59$ Å, building up *chains* arranged over the ab plane in a triangular lattice, with a much larger spacing (interchain distance $a/\sqrt{3} = 5.24$ Å).[1,2] The Co^{3+} oxidation state at both sites is now established,[3,4] contrary to earlier predictions for a Co^{2+}-Co^{4+} charge disproportionation.[5]

Magnetism resides on the Co II site, where a trigonal crystal field yields a high-spin ground state with a large unquenched orbital component ($\langle L_z\rangle \approx 1.7$, $\langle 2S_z + L_z\rangle = 5.3$), while Co I is in a low-spin state (i.e., nonmagnetic).[3] Spin-orbit coupling gives rise to a single-ion anisotropy term $-DS_z^2$ of order 70 meV (corresponding to an anisotropy field $B_{\rm anis} \approx 200$ T along c), whence the strong Ising-type character of magnetism in this system.[2,6] Exchange coupling between the Co^{3+} II ions is ferromagnetic (FM) and relatively strong along the chains,[7] whereas it is antiferromagnetic (AF) and much weaker between chains. While the dominant intrachain exchange interaction promotes quasi-one-dimensional Ising-type ferromagnetism, the actual magnetic structure is the result of the competing residual interchain AF coupling, giving rise to a complex magnetic phenomenology as a function of temperature and magnetic field.

Susceptibility measurements actually demonstrate the onset of magnetic order at $T < T_c \approx 25$ K.[2,8] The nature of the magnetic ordering however, has been the subject of a long-lasting controversy. Denoting spin-up, spin-down, or magnetically disordered Ising chains as ↑,↓, 0, respectively, theoretical models indicated either a ferrimagnetic (FI) [↑ ↑ ↓] or a partially disordered antiferromagnetic (PDA) structure [↑ ↓ 0] as the stable zero-field arrangement of the three inequivalent chains on the triangular lattice in the presence of geometrically frustrated AF interchain coupling.[9,10] Early neutron diffraction experiments seemingly supported either a PDA (Refs. 11,12) or a FI (Ref. 8) order, although poor quantitative agreement of both structures with magnetic peak intensities was later pointed out.[13] Recent x-ray[14] and neutron scattering[15] data on single crystals have revealed the incommensurate character of the magnetic order in this compound. They show that the actual structure, referred to as *modulated PDA* (MPDA), rather consists of long-wavelength longitudinal spin-density modulations along each chain, phase shifted by $\pm 2\pi/3$ with respect to the neighboring chains.[15] Nevertheless, the MPDA

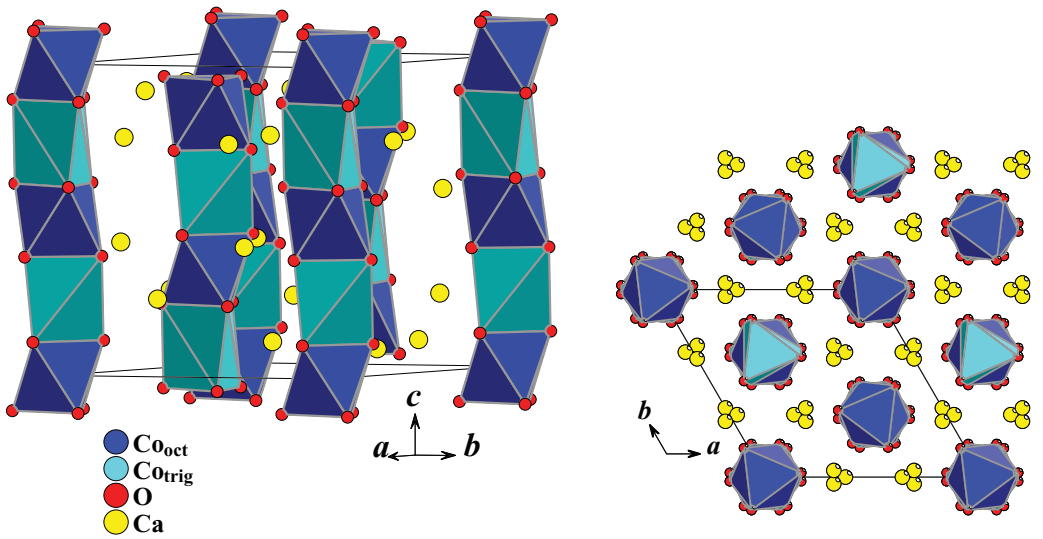

FIG. 1. (Color online) Lattice structure of $Ca_3Co_2O_6$ in the hexagonal setting. Left: perspective view of the spin chains formed by the CoO_6 polyhedra along the c axis; right: cross section in the ab plane, evidencing the arrangement of chains in the triangular lattice. The dark and light polyhedra represent the CoO_6 octahedra and CoO_6 trigonal prisms, respectively.

phase is apparently metastable below 14 K, as indicated by the decrease in the intensity of the MPDA magnetic peaks.[13–15]

The nature of the magnetic order in an externally applied magnetic field is also far from clear. Increasing magnetic fields applied along c tend to stabilize the FI phase and eventually FM interchain order.[2,11] At $5\ \mathrm{K} < T < T_c$, the initial saturation of the magnetization to a magnetic moment $M_{\mathrm{FI}} \approx 1.7\mu_B$ per formula unit at $\mu_0 H > B_{c1} \approx 0.1\ \mathrm{T}$, followed by a step to $M_{\mathrm{FM}} \approx 3M_{\mathrm{FI}}$ at $\mu_0 H > B_{c2} \approx 3.5\ \mathrm{T}$, actually points to perfect FI and FM phases below and above H_{c2}, respectively. However, the $M(H)$ curves at lower temperatures display a puzzling multistep behavior reminiscent of the quantum tunneling of magnetization detected in molecular magnets.[16,17] A number of complex magnetic superstructures, distinct from both the FI and FM spin-chain arrangements, have been proposed in order to explain the fractional magnetization values. However, such superstructures cannot account for all the plateaus observed in $M(H)$.[18]

In this paper, we address the issue of the field-dependent magnetic order of $Ca_3Co_2O_6$ by means of ^{59}Co nuclear magnetic resonance (NMR) in a variable external field. Previous ^{59}Co NMR research on $Ca_3Co_2O_6$ polycrystalline samples, though successful in demonstrating the presence of nonmagnetic Co^{3+}, could only provide very limited information on the magnetic structure, due to the powder averaging of the complex multiline quadrupolar spectra,[4] while a more recent single-crystal NMR study showed the dependence of the sharp peaks on the sample orientation in a large external magnetic field, but, due to the fixed intensity of the latter, it could not properly address the metamagnetic transitions.[19] The FM and FI surroundings, on the contrary, can be clearly resolved in our NMR investigation of a high-quality single crystal in a field-sweeping environment, while the two field-induced transitions, namely, MPDA-FI and FI-FM, were precisely identified at 10 K through steplike jumps in the internal field and peculiar features of the spin-spin relaxations, indicative of glassy spin dynamics. Our study also yields a detailed characterization of the chemical shift and the electric field gradient (EFG) tensors at the nonmagnetic Co I site.

The paper is organized as follows. Sample preparation and the experimental methods are briefly described in Sec. II. NMR spectra, providing information on the magnetic structures, and nuclear relaxation data, probing the dynamical excitations of the spin system, are presented in Secs. III A, and III B, respectively. The calculated dipolar fields at the Co I sites in the FI and FM phases are compared with experimental values in Sec. IV. The results are discussed in Sec. V. Two appendixes review in some detail the complex dependence of the ^{59}Co resonances on magnetic and quadrupolar interactions, and the longitudinal relaxation function of a 7/2 nuclear spin.

II. EXPERIMENT

The investigated sample was a single crystal of size $1.2 \times 1.2 \times 5.8\ \mathrm{mm}^3$ (the long side parallel to the c axis) taken from a batch of several needle-shaped crystals obtained by the flux method. The crystals were grown using the following procedure: a mixture of $Ca_3Co_2O_6$ powder and KCO_3 (the flux), in a weight ratio 1/7, was heated up to 990 °C in an alumina crucible for 1 h and then slowly cooled down to room temperature. A sample of the same batch was employed for the resonant x-ray scattering study of Ref. 14. The high quality of the crystals was confirmed by preliminary x-ray diffraction, energy-dispersive x-ray, magnetization, and specific heat measurements.

Magnetization measurements were performed after zero-field cooling, by using a vibrating-sample magnetometer (Oxford Instruments) equipped with a 12 T magnet, with a field sweep rate of 1 T/min in order to minimize any relaxation effect. Susceptibility measurements were carried out by means of a superconducting quantum interference device (SQUID) magnetometer with magnetic fields up to 5 T and temperatures down to 1.8 K (Quantum Design MPMS). The magnetic measurements were carried out for the two

geometries corresponding to the magnetic field applied parallel or perpendicular to the c axis, i.e., parallel or perpendicular the direction of the chains and the spins. In the case of parallel geometry the crystals were aligned using the magnetic field itself at 5 T as explained in Ref. 20. The alignment of the crystals in the perpendicular geometry can be easily obtained thanks to their rodlike shape.

The NMR experiments were performed by means of a home-built phase-coherent pulsed spectrometer[21] and a fast-sweeping cold-bore cryomagnet (Oxford Instruments EXA) equipped with a variable-temperature insert as a sample environment. The crystal was mounted on a sample rotator, providing an angular span of $\pm 120^\circ$ with respect to the applied field. Misalignment of the rotation axis (nominally perpendicular to the field) was estimated not to exceed 5°. In the case of the c axis parallel to the field, however, a precise alignment of the sample was achieved, thanks to its large magnetic anisotropy, by loosely mounting it in the coil.

NMR spectra were detected by exciting spin echoes by means of a standard P-τ-P sequence, with equal rf pulses P of duration 3–5 μs and intensity suitably regulated for optimum signal, and delays τ kept as short as possible with respect to the dead time of the resonant probe head ($\approx$10–25 μs depending on the working frequency). Recording was carried out either by tuning the probe head at discrete frequencies in a constant field (frequency-sweep mode), or by varying the applied field and exciting the resonance at a constant frequency (field-sweep mode). Although an indirect method, we preferentially employed the latter whenever possible (namely, far from the metamagnetic transitions) as it yields smoother data, independent of the frequency response of the spectrometer, in a fully automated procedure.

Nuclear spin-spin relaxations were determined by the decay of the signal amplitude in the same spin echo sequence P-τ-P, as a function of variable delay τ. Spin-lattice relaxations were measured by the signal recovery following a so-called fast saturation of the observed nuclear transition (see Appendix B), obtained with an aperiodic train of 10–15 pulses.

III. EXPERIMENTAL RESULTS

A. NMR spectra

We report separately the ^{59}Co resonance spectra recorded in the longitudinal geometry (external field $\boldsymbol{B}_{\rm ext} \parallel c$ axis), a geometry that allowed us to study the field-induced magnetic order in the system, and in transverse applied fields. Interpretation of the spectra is relatively simple and model independent in the longitudinal case thanks to the collinearity of the internal magnetic field and the EFG with the c axis, since the latter is both the easy magnetization direction and a local high-symmetry axis for Co I.[1,13] In the general case, the dependence of the ^{59}Co resonances on magnetic and quadrupolar interactions is rather complex, as is recalled in some detail in Appendix A.

1. Longitudinal applied fields

A ^{59}Co NMR signal could be detected below 15 K in moderate longitudinal external magnetic fields $B_{\rm ext} > 0.1$ T. For such field values the FI phase is induced in the system. In contrast, no signal could be detected in the MPDA phase at $B_{\rm ext} < 0.1$ T.

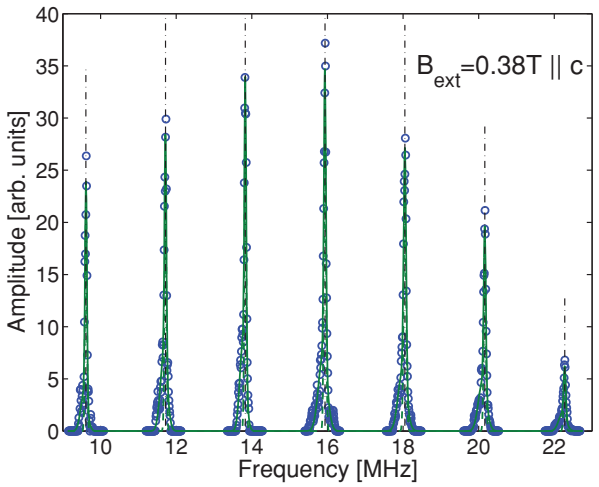

FIG. 2. (Color online) Frequency-swept ^{59}Co spectrum at 10 K from the majority spin-up chains of the FI phase, recorded in a field of 0.38 T applied along the c axis. The plotted amplitude is corrected for the frequency-dependent sensitivity $\propto \nu^2$. Solid lines are bimodal fits of the satellite peaks; vertical dash-dotted lines mark their centers of gravity.

A typical frequency-sweep spectrum, recorded at 10 K in 0.38 T, is plotted in Fig. 2. The spectrum consists in a septet of quadrupole-split Zeeman transitions ν_n, $n = -3, \ldots, n = 3$ [Eq. (A2)], with constant frequency spacing $\nu_{n+1} - \nu_n = 2.11(1)$ MHz, in agreement with Ref. 19. In this geometry ($\theta = 0$), and in the presence of a cylindrical EFG ($\eta = 0$), as is actually the case (see Sec. III A 2), such a line spacing coincides with the quadrupolar coupling parameter ν_Q [Eq. (A3)]. The resonance frequency ν_0 of the central line, which is unaffected by the quadrupole interaction, corresponds to a field $B_{\rm nuc} = 2\pi\nu_0/{}^{59}\gamma$ at the nucleus, which is larger than $B_{\rm ext}$ by approximately 1.2 T (here, ${}^{59}\gamma = 2\pi \times 10.10$ MHz/T is the gyromagnetic ratio[22] of ^{59}Co). Such a field offset, though sizable, is nevertheless much smaller than the typical hyperfine fields detected in magnetic Co^{3+}, which are of the order of -10 T/μ_B and $+60$ T/μ_B for the spin and orbital hyperfine components, respectively.[23,24] This confirms that the present ^{59}Co signals are from Co^{3+} ions in a low-spin state, in agreement with previous NMR reports.[4,19] We note that the dipolar field at site I generated by two nearest-neighbor Co II moments of the order of 5.2 μ_B (as determined from magnetization measurements) aligned parallel to $\boldsymbol{B}_{\rm ext}$ accounts for both the positive sign of the field offset $B_{\rm nuc} - B_{\rm ext}$ and its magnitude to within a few percent accuracy. This is the first indication that the internal field $\boldsymbol{B}_{\rm int} \approx \boldsymbol{B}_{\rm nuc} - \boldsymbol{B}_{\rm ext}$ arises from the surrounding magnetic ions essentially through the dipolar coupling, as actually proven in detail by the internal field calculations of Sec. IV. Given its dominant on-chain dipolar origin, the positive sign of $B_{\rm int}$ then indicates that the nearest-neighbor Co^{3+} spins are aligned along the direction of the applied field. The present positive-offset line multiplet therefore originates from nuclei at the Co I sites of spin chains aligned parallel to the external field, namely, the majority chains of the FI structure.

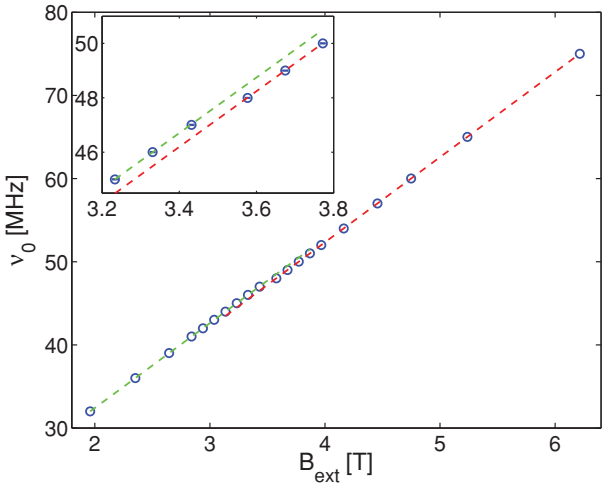

FIG. 3. (Color online) Central resonance frequency ν_0 of the positive-offset spectra from the spin-up chains in either the FI ($B_{\rm ext} < 3.5$ T) or the FM phase ($B_{\rm ext} > 3.5$ T), as a function of $\boldsymbol{B}_{\rm ext} \parallel c$. The dashed lines are fits to straight lines for the two phases. The inset is an enlargement of the transition region.

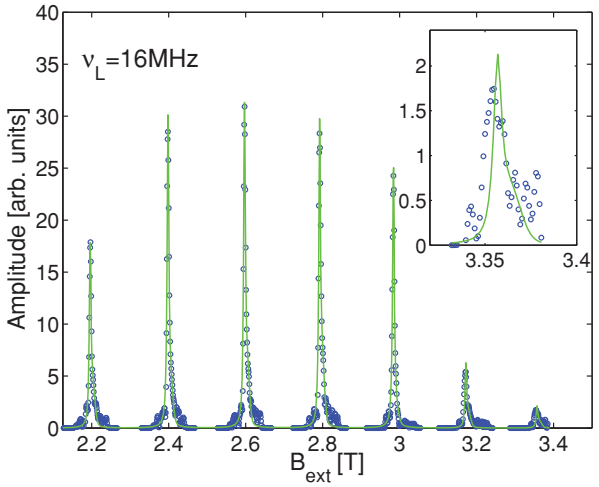

FIG. 4. (Color online) Field-swept spectrum ($\boldsymbol{B}_{\rm ext} \parallel c$) at 10 K from the minority spin-down chains, recorded at a constant frequency $\nu = 16$ MHz. The solid line is a bimodal fit to a septet of quadrupolar satellites, with positions constrained by Eq. (A2). The inset is an enlargement of the rightmost satellite at $B_{-3} \approx 3.36$ T.

Qualitatively similar positive-offset spectra could be reproduced in increasing external fields parallel to the c axis at 10 K, up to $B_{\rm ext} = 3.5$ T. The resonance frequency of the central line follows a linear dependence on $B_{\rm ext}$ (Fig. 3),

$$\nu_0 = a B_{\rm ext} + b, \tag{1}$$

with best-fit parameters $a_\uparrow = 10.21(1)$ MHz/T, $b_\uparrow = 12.02(2)$ MHz (hereafter, $\uparrow$ and $\downarrow$ in the subscripts denote quantities related to spin-up majority and spin-down minority chains of the FI phase, respectively). On the other hand,

$$2\pi\nu_0 \equiv {}^{59}\gamma B_{\rm nuc} = {}^{59}\gamma(1 + K_c)(B_{\rm ext} + B_{\rm int}) \tag{2}$$

as detailed in Appendix A. If the staggered magnetization is saturated all over the field span, the internal field $\boldsymbol{B}_{\rm int}$ is independent of $B_{\rm ext}$ and, by symmetry, also parallel to c. Working under this hypothesis, whose validity is demonstrated in the discussion, a comparison of Eqs. (1) and (2) simply relates the coefficients a and b to $B_{\rm int}$ and the c axis component of the chemical shift tensor K_c: $a = {}^{59}\gamma(1 + K_c)/(2\pi)$ and $b = {}^{59}\gamma(1 + K_c)B_{\rm int}/(2\pi)$, respectively. Best-fit values for $a_\uparrow$ and $b_\uparrow$ then yield $B_{{\rm int}\uparrow} = 1.178(2)$ T, and a sizable $K_c \approx 0.01$.

Resonances from the minority spin-down chains are marked by a negative field offset, comparable in absolute value to the internal field in the majority chains. The signal could only be found in longitudinal fields exceeding 2 T, since for smaller external fields its resonance frequency $\nu_0 \approx {}^{59}\gamma||B_{\rm int}| - |B_{\rm ext}||/(2\pi)$ falls below 10 MHz, outside the frequency range of our apparatus. A field-sweep spectrum at 10 K, recorded at fixed frequency of 16 MHz, is shown in Fig. 4. It consists of a multiplet of quadrupole-split lines centered at B_n,[25] similar to those detected for the majority chains, with a central resonance at $B_0 = 2.792$ T. The two satellites at $B_{-2} = 3.172$ T and $B_{-3} \approx 3.36$ T are however reduced in amplitude by approximately 75% and 90% with respect to the symmetric peaks at B_2 and B_3, respectively. The signal loss at $B_{\rm ext} \geqslant B_{-2}$ is due to the approach of the FI-FM transition at $B_{c2} \approx 3.5$ T, which is accompanied by a notable relaxation phenomenon that partially wipes out the signal intensity over a wide field interval close to B_{c2} (see below). The rightmost satellite at B_{-3} is furthermore displaced from the expected position by approx. -2 mT (figure inset), a value well accounted for by the demagnetization field, since the macroscopic magnetization significantly deviates from the FI plateau at $H = \mu_0^{-1} B_{-3}$ (Fig. 12). The quadrupole coupling parameter is estimated as $\nu_Q = 1.97(1)$ MHz from the line spacing, $2\pi\nu_Q = {}^{59}\gamma(1 + K_c)(B_{n-1} - B_n)$, and is slightly, but significantly smaller than in the spin-up chains.

The resonance frequency of the central line follows a similar linear dependence on $B_{\rm ext}$ (Fig. 5), with slope $a_\downarrow = 10.22(1)$/MHz/T, and a negative intercept $b_\downarrow = -12.48(3)$ MHz [Eq. (1)]. The former coincides within error with $a_\uparrow$, whence the same chemical shift value $K_c \approx 0.01$ is

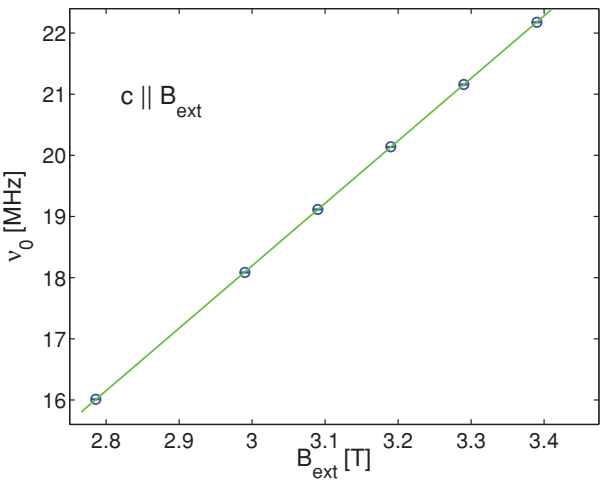

FIG. 5. (Color online) Central resonance frequency ν_0 of the spectra from the minority spin-down FI chains, as a function of $\boldsymbol{B}_{\rm ext} \parallel c$. The solid line is a fit to Eq. (1).

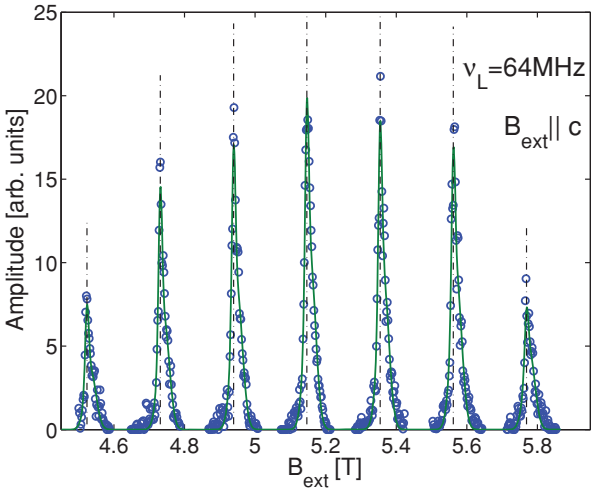

FIG. 6. (Color online) Field-swept ($\boldsymbol{B}_{\rm ext} \parallel c$) ^{59}Co spectrum in the FM phase at 10 K, recorded at a constant frequency $\nu = 64$ MHz. Solid lines are bimodal fits of the satellite peaks; vertical dash-dotted lines mark their centers of gravity.

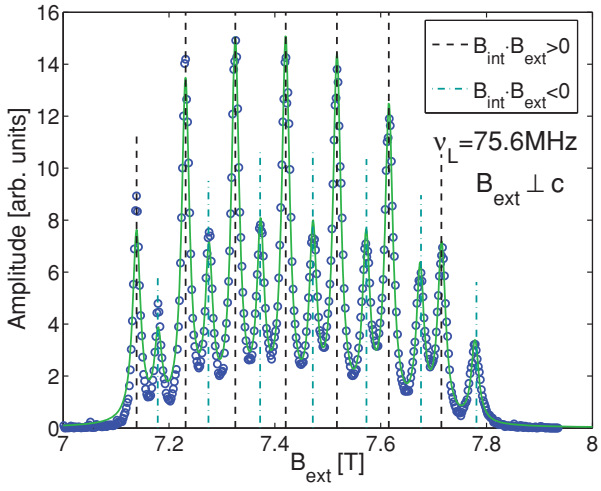

FIG. 7. (Color online) Field-swept spectrum at 10 K, recorded at a constant frequency of 75.6 MHz, in a nominally transverse geometry ($\boldsymbol{B}_{\rm ext} \perp c$). The solid line is a global fit to two septets of Lorentzian lines with positions constrained by Eq. (A2). Vertical dashed and dash-dotted lines mark peak positions for the majority and minority spin-chain signals, respectively.

obtained. From $b_{\downarrow}$, the internal field at Co I in the minority chains is estimated as $B_{\rm int\downarrow} = -1.221(4)$ T.

The negative-offset resonance lines from the minority spin-down chains completely disappear in external fields $B_{\rm ext} > 3.5$ T, while only a positive-offset septet can be detected, that is qualitatively similar to the one from the majority FI chains below 3.5 T and with an identical quadrupole splitting $\nu_Q = 2.11(1)$ MHz (Fig. 6). The integrated amplitudes of the positive-offset spectra above and below 3.5 T, and proportional to the number of ^{59}Co nuclei excited in spin-up chains, have a ratio very close to 3:2. These facts indicate that all the spin chains are now aligned parallel to the external field, i.e., the system is in a FM state.

The positive-offset septet from the spin-up chains could be followed at 10 K while increasing $B_{\rm ext}$ in steps of approx. 0.1 T across the field-induced FI-FM transition, without losing the signal. The resonance frequency of the central line is plotted vs $B_{\rm ext}$ in Fig. 3. Experimental points clearly follow two different straight lines above and below 3.5 T [Eq. (1)], which signals the occurrence of a transition at a critical field $B_{c2} = 3.50(5)$ T. Line parameters on the FM side are fitted as $a^{\rm FM} = 10.23(1)$/MHz/T, in good agreement with the a values in the FI phase, and a reduced $b^{\rm FM} = 11.40(1)$ MHz, corresponding to a steplike decrease of the internal field $B_{\rm int}^{\rm FM} = 1.115(2)$ T.

The transition is also accompanied by an abrupt broadening by a factor of about 2 of the satellite lines above B_{c2}. A closer inspection of the resonance lines reveals, on both sides of the transition, an asymmetrical bimodal shape with a sharper peak and a broader negatively shifted shoulder, that is more pronounced in the FM phase. Line shapes and widths, in contrast, are independent of satellite order m. These facts indicate that the observed inhomogeneous broadening is magnetic in origin. The increase in linewidth $\Delta\nu_L$ above B_{c2} qualitatively agrees with a dominant line broadening from the demagnetization field, which is proportional to the net magnetic moment, and inhomogeneous throughout the sample due to its nonellipsoidal shape. The agreement is not quantitative, however, since a step in $\Delta\nu_L$ by a factor of 3 across B_{c2} is expected from the corresponding step in the macroscopic magnetization. Such a discrepancy suggests the presence of an extra broadening mechanism, relatively more important in the FI phase.

2. *Transverse applied fields*

The crystal was also mounted with its c axis perpendicular to the external field, in order to study the transverse components of the EFG and $\hat{K}$ tensors in an azimuthal scan of $\boldsymbol{B}_{\rm ext}$ in the ab plane. A typical field-sweep spectrum at 10 K, recorded at a fixed frequency $\nu_L = 75.6$ MHz, is shown in Fig. 7. The spectrum consists of two septets of relatively sharp quadrupole-split transitions, with positive ($B_0 < 2\pi\nu_L/^{59}\gamma$) and negative ($B_0 > 2\pi\nu_L/^{59}\gamma$) offsets of their respective central lines. The integrated amplitudes of the positive- and negative-offset multiplets are in a ratio very close to 2. Following the above arguments, the two multiplets originate from the majority spin-up and minority spin-down chains, respectively, in the presence of a sample misalignment of the order of a few degrees, yielding a longitudinal field component of order a few hundreds of millitesla, strong enough to induce FI magnetic order in the sample.[26] The effect of sample rotation around an axis nominally coincident with the crystallographic c axis is summarized in Fig. 8, showing the dependence on the azimuthal angle ϕ of the central lines $B_{0\uparrow}$, $B_{0\downarrow}$, and of the first-order quadrupole splittings, calculated as $(B_{-1} - B_1)/2$ (in field units).[25] Overlaid on the experimental points, the figure also shows for comparison simulated splittings [Fig. 8(a)] and shifts [Fig. 8(b)] predicted by Eqs. (A2) and (A3) for $\theta = 81^\circ$ (the angle between c and $\boldsymbol{B}_{\rm nuc} \approx \boldsymbol{B}_{\rm loc}$, resulting from a vector addition of $B_{\rm ext} = 7.45$ T with a perpendicular $B_{\rm int} \approx 1.2$ T), and rhombicity factors η of order 0.1 reproducing the experimental absolute variation in quadrupole splitting. Clearly, the experimental splittings and shifts do not follow the predicted angular periodicity of

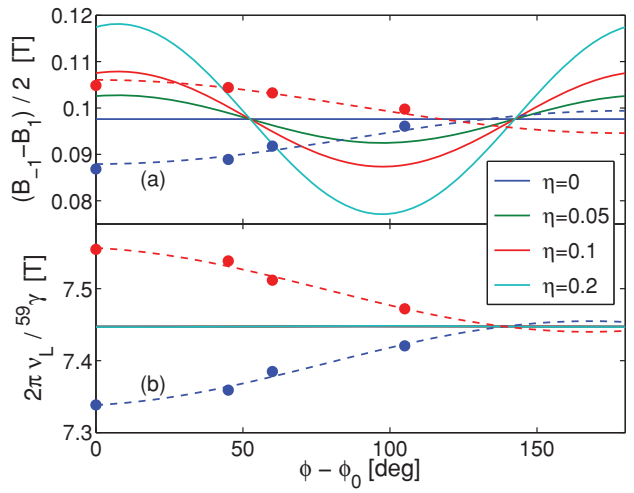

FIG. 8. (Color online) Symbols: experimental first-order quadrupole splitting (a) and central peak position (b), in field units, as a function of the azimuthal angle ϕ in the transverse geometry. Dashed lines are guides to the eye. Solid lines: simulations with $\theta = 81^\circ$, corresponding to $\boldsymbol{B}_{\rm ext} \perp c$ [see text and Eq. (A2)], for increasing η values.

π, rather showing a 2π period [Fig. 8(a)], as in the case of a simultaneous misalignment of the rotation axis from both the c axis and the plane perpendicular to $\boldsymbol{B}_{\rm ext}$. Moreover, the quadrupolar shift is negligible even for large η values [Fig. 8(b)], since it is a second-order term in ν_Q/ν_Z. Therefore, the magnitude and the azimuthal dependence of both quantities are fully justified solely by misalignment. This sets an upper limit to η of a value of order 0.01, much smaller than the plotted η values. Such a limit may be regarded as the evidence, within experimental accuracy, for a cylindrical EFG at Co I with a principal axis coincident with c, in agreement with symmetry arguments.

The data of Fig. 8 are obtained by the fit of each spectrum to two septets of Lorentzian lines (Fig. 7) with constrained positions calculated as functions of external and internal fields, chemical shift, quadrupole interaction ($\eta = 0$), and the geometric angle α between the c axis and $\boldsymbol{B}_{\rm ext}$. In the fit, the in-plane chemical shift tensor component $K_a \equiv K_b$, α, and $\nu_{Q\uparrow}$, $\nu_{Q\downarrow}$ (which are in principle independent for the two chain types) were treated as free variational parameters, while $B_{{\rm int}\uparrow}$, $B_{{\rm int}\downarrow}$, and K_c were kept fixed to the values determined by NMR in the longitudinal geometry. A further constant parameter, $\rho \equiv d\psi/dB_{\rm ext} = \chi_\perp/\mu_s$, accounting for a field-dependent tilting angle ψ of the electronic moments, was calculated as $\rho = 3.4(2) \times 10^{-3}$ T^{-1} from the ab-plane macroscopic susceptibility, determined by SQUID magnetometry as $\chi_\perp = 1.8(1)\times 10^{-2}\,\mu_B$/T (here $\mu_s \approx 5.2\,\mu_B$ is the saturation magnetic moment per Co II ion). The best-fit values of α range in the 85°–88.5° interval, which ensures that $B_{\rm ext}\cos\alpha \geqslant 0.2$ T $> B_{c1}$ in all cases, in agreement with the FI order. The fits consistently yield a negative $K_a = -6.7(2) \times 10^{-3}$ independent of ϕ,[27] and $\nu_{Q\uparrow} = \nu_{Q\downarrow} = 2.11(1)$ MHz, coincident with the quadrupole line splitting of the majority signal in the longitudinal geometry, and so in disagreement with the value determined for the minority chains in large longitudinal fields.

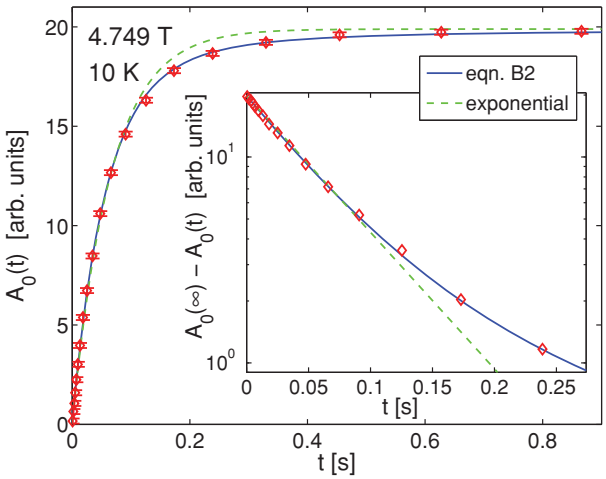

FIG. 9. (Color online) Recovery of the signal amplitude A_0 of the central line (10 K, longitudinal $B_{\rm ext} = 4.749$ T) following a fast saturation of nuclear transition, as a function of the delay t between the saturating pulse train and the spin-echo detection. The solid and dashed lines are best fits to the multiexponential law of Eq. (B2) and a single-exponential recovery $A_0(t) = A_0(\infty)[1 - \exp(t/T_1))]$, respectively. Inset: semilogarithmic plot of $A_0(\infty) - A_0(t)$, evidencing the nonexponential behavior.

B. Nuclear relaxations

Nuclear relaxations were systematically studied on the central quadrupole line ($n = 0$) in the longitudinal geometry ($\boldsymbol{B}_{\rm ext} \parallel c$) at 10 K as a function of the external field. The longitudinal nuclear polarization recovers equilibrium in good agreement with Eq. (B2) (Fig. 9), indicating that spin-lattice relaxations are actually driven by magnetic fluctuations, as expected in this system.

Figure 10(b) (open symbols) displays spin-lattice and spin-spin relaxation rates of the positive-offset septet at 10 K over the 2–6 T field span for $\boldsymbol{B}_{\rm ext} \parallel c$, an interval comprising the FI-FM transition B_{c2}. Spin-spin rates T_2^{-1} are larger than spin-lattice rates $T_1^{-1} \equiv 2W$ [Eq. (B2)] by at least three orders of magnitude, and the two relaxations clearly follow quite different behaviors vs $B_{\rm ext}$. The former exhibits a peak at B_{c2}, with such a large maximum value that it nearly leads to the disappearance (wipeout) of the signal at this temperature. In contrast, T_1^{-1} exhibits a monotonic decrease with increasing fields, except for a shallow feature at B_{c2}. Moreover, the time dependence of the spin-spin relaxations exhibits a marked nonexponential decay over a wide field interval across the FI-FM transition. The signal decay is best fitted to a stretched exponential function $A(\tau) = A_0 \exp[-(2\tau/T_2)^\beta]$, with stretching exponent β peaked to a value of 1.5 at B_{c2}, i.e., the intrinsic line shape (related to the spin-spin relaxation function by Fourier transform) is nearly Gaussian close to the transition.

The difference in magnitude and field dependence of the T_1^{-1} and T_2^{-1} rates is not peculiar to the longitudinal orientation. It can be qualitatively reproduced, in fact, with the c axis rotated by $\alpha = 45^\circ$ in $B_{\rm ext} = 4$–8 T [filled symbols in Fig. 10(b)], a field interval encompassing the FI-FM transition in that geometry, if we except a moderate increase in T_1^{-1} by a factor of 5. This indicates that the behavior of T_1^{-1} and

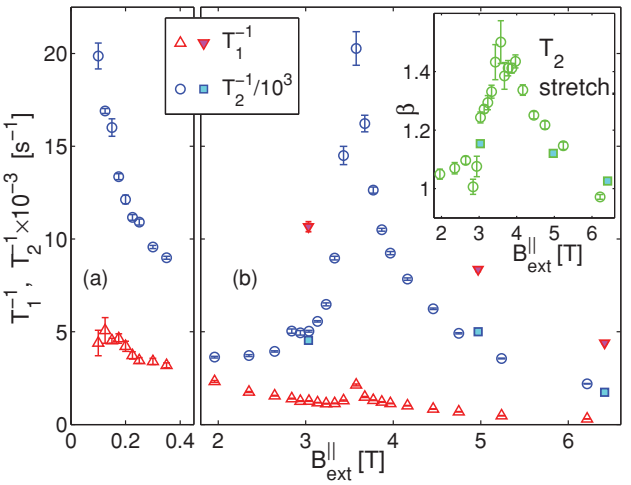

FIG. 10. (Color online) Spin-lattice (triangles) and spin-spin relaxations (bullets and squares) measured on the central resonance of the positive-offset septet at 10 K as a function of the parallel component $B_{\rm ext}^{\parallel} \equiv \cos\alpha B_{\rm ext}$ of the external field, for $\boldsymbol{B}_{\rm ext} \parallel c$ (open symbols) and with the c axis rotated by $\alpha = 45^\circ$ (filled symbols), (a) on approaching the FI-MPDA transition from above, and (b) across the FI-FM transition. Inset of (b) stretching exponent β of the spin-spin relaxation function vs $B_{\rm ext}^{\parallel}$. In the figure T_2^{-1} rates are scaled by a multiplication factor of 10^{-3} for clarity.

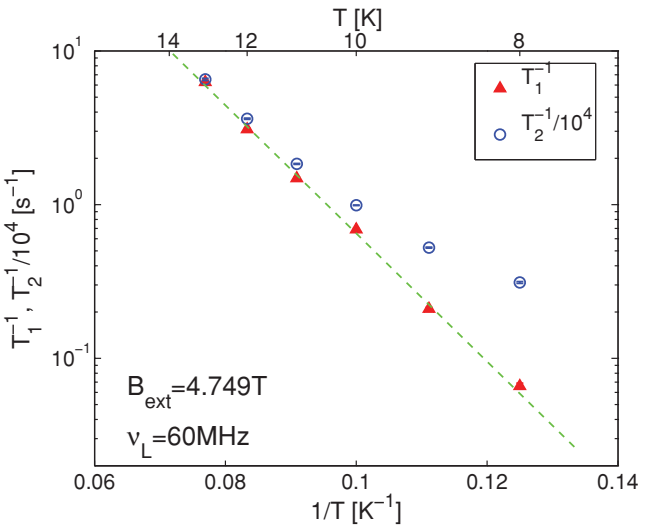

FIG. 11. (Color online) Spin-spin (bullets, rescaled) and spin-lattice relaxation rates (triangles) measured in the FM phase on the central resonance ($\nu_0 = 60$ MHz, $\boldsymbol{B}_{\rm ext} = 4.749$ T parallel to c) as a function of temperature. The dashed line is a fit of T_1^{-1} to an Arrhenius law. In the figure T_2^{-1} rates are scaled by a multiplication factor of 10^{-4} for clarity.

T_2^{-1} vs applied field is essentially invariant with respect to the orientation of the nuclear field $\boldsymbol{B}_{\rm nuc} \approx \boldsymbol{B}_{\rm loc}$ relative to the c axis (note that $B_{\rm ext} \gg B_{\rm int}$ in this case, so that the $\boldsymbol{B}_{\rm loc}$ direction is approximately that of $\boldsymbol{B}_{\rm ext}$).

Perfectly consistent data are recorded from nuclei in the minority spin-down chains, for $B_{\rm ext}$ approaching B_{c2} from below. A qualitatively similar behavior of the two kinds of relaxations is also observed at 10 K close to the other metamagnetic transition, i.e., from the FI to the MPDA phase on decreasing the longitudinally applied $B_{\rm ext}$ down to $B_{c1} \approx 0.1$ T [Fig. 10(a)]. Here again T_2^{-1} is orders of magnitude larger than T_1^{-1} and increases as $B_{\rm ext}$ approaches the critical field, while T_1^{-1} is nondivergent. As in the vicinity of B_{c2}, the intrinsic line shape is quasi-Gaussian, as spin-spin relaxations are fitted to stretched-exponential decay forms, with β in the range 1.2–1.4.

Spin-lattice relaxations were also measured as a function of temperature and applied field, in both the FI and FM phases. Results of a typical temperature scan, performed in a longitudinal field of 4.749 T (i.e., in the FM phase) are shown in Fig. 11. The figure also shows the temperature dependence of T_2^{-1} for comparison. The spin-lattice rate clearly follows a thermally activated behavior $T_1^{-1} = T_\infty^{-1} \exp -\Delta/T$, as also found by other authors.[19] The Arrhenius law is obeyed over a temperature range of 8–13 K at this particular field, corresponding to a T_1 variation by more than two decades, with activation energy estimated as $\Delta = 96(2)$ K. Above this temperature interval the signal is lost due to an exceedingly short T_2, while experimental T_1^{-1} points exhibit excess relaxation at $T < 8$ K, indicating that the relaxation mechanism responsible for the Arrhenius behavior becomes unimportant at low temperature, and it is shunted by other more effective relaxation channels. Spin-spin rates seemingly saturate at low temperature and also exhibit a steep temperature dependence at $T > 8$ K as well, although the evolution is clearly not Arrhenius-like.

Thermally activated $T_1^{-1}(T)$ were detected at *all fields*, irrespective of whether the system exhibits FI or FM order. The field dependence of the activation energy $\Delta(B_{\rm ext})$, as well as its interpretation in terms of the elementary excitations of an Ising spin-chain system, will be reported elsewhere.

IV. DIPOLAR FIELD CALCULATION

A calculation of the total dipolar field at the Co I site is required for a quantitative analysis of our experimental internal field values. We report such a calculation here for each of the three magnetic environments, majority FI-, minority FI-, and FM-ordered chains. The contribution of nearby moments (referred to as the proper dipolar field $B_{\rm dip}$) is calculated by summing up the individual dipolar fields from Co II spins $\boldsymbol{S}_j$ at positions $\boldsymbol{r}_j$ inside a Lorentz sphere with a radius of several unit cells centered at a Co I site $\boldsymbol{r}_0 = \boldsymbol{0}$, $\boldsymbol{B}_{\rm dip} = \sum_j g\mu_B(3\boldsymbol{r}_j\boldsymbol{r}_j \cdot \boldsymbol{S}_j - r_j^2\boldsymbol{S}_j)/r_j^5$, while spins outside the Lorentz sphere are treated as a macroscopic magnetic moment density, giving rise to a demagnetization field $B_{\rm dem}$ inside the sphere, as is customary. The latter is strictly constant throughout the sample volume only in the case of an ellipsoidal sample surface, whereby it is simply proportional to the saturation magnetization M_s and to the difference in demagnetizing factors of the inner Lorentz sphere 1/3 and the outer sample surface N, $B_{\rm dem} = 4\pi\,(1/3 - N)M_s$. For a rotational ellipsoid magnetized along its principal axis c, the demagnetizing factor N_c is calculated as[28]

$$N_c = \frac{(1-\epsilon^2)(\tanh^{-1}\epsilon - \epsilon)}{\epsilon^3}, \qquad \epsilon \equiv \sqrt{1-(r_a/r_c)^2}. \tag{3}$$

TABLE I. Calculated dipolar sum $B_{\rm dip}$, demagnetization field $B_{\rm dem}$, and total dipolar field $B_{\rm tot} \equiv B_{\rm dip} + B_{\rm dem}$ as a function of magnetic chain ordering, compared with experimental $B_{\rm int}$ values.

Order	$B_{\rm dip}$ (T)	$B_{\rm dem}$ (T)	$B_{\rm tot}$ (T)	Expt. (T)
FM	0.997	0.137	1.134	1.115(2)
FI↑	1.122	0.046	1.167	1.178(2)
FI↓	−1.246	0.046	−1.201	−1.221(4)

A nonellipsoidal sample may be approximated by an effective ellipsoid accounting for the mean $B_{\rm dem}$, while deviations from the ideal shape gives rise to a distribution in demagnetization fields, contributing only to the linewidth. We assume effective ellipsoid radii $r_a = r_b$, r_c equal to half of the sides of our square-base parallelepipedal specimen as a best ellipsoidal approximation. The choice of r_a and r_c does not critically affect the determination of $B_{\rm dem}$, since N_c depends weakly on ϵ in the case of an elongated sample (e.g., $\partial N_c/\partial\epsilon \approx 0.3$ for our crystal). For instance, a 10% error on ϵ would result in an error $\Delta B_{\rm dem}$ of order 5 and 2 mT in the FM and FI phases, respectively.

The results of our calculations are summarized in Table I and compared with experimental results. Both the dipolar sums and the demagnetization field were calculated by assuming the Co II moments saturated to $\pm g\langle S_z\rangle \mu_B$ along c in all the three types of magnetic chains, with a $\pm$ sign as appropriate for the chain order, and identical absolute moment values estimated as $g\langle S_z\rangle = 5.25(3)$ (in units of μ_B) from an extrapolation of $M(H)$ data in high field. Lattice parameters were taken as $a = 9.061$ Å, $c = 10.367$ Å as reported in the literature at 40 K.[1] Numerical convergence of $B_{\rm dip}$ could be attained with a Lorentz sphere radius of the order of 30 unit cells. Calculated and experimental values differ by less than 2% in all cases. Agreement should be considered satisfactory in view of the uncertainties in the magnetic moment (of order 1%) and the demagnetization factor. This confirms that the internal field is dipolar in origin, while transferred hyperfine contributions, if they occur, are negligible.

V. DISCUSSION AND CONCLUSIONS

We organize the discussion of our experimental results into separate sections for the sake of clarity, each one focusing on one main conclusion of the paper.

A. Interactions of ^{59}Co: evidence against a direct Co I-Co II superexchange path

Our NMR study on a single-crystal provides a determination of the chemical shift and the EFG tensors at the Co I site. The chemical shift is less precise due to the uncertainty in the zero-shift ^{59}Co reference[29] and to the presence of a large internal field which complicates the unraveling of $\hat{K}$ components (see Appendix A). The absolute magnitude of K, of order 1%, though sizable in absolute terms, is however only slightly larger than the typical values reported for diamagnetic complexes of cobalt.[30] The relatively small value of K agrees with the known large crystal-field splitting at the octahedral I site, of order 0.65 eV,[3] since a near-lying crystal-field-excited multiplet usually gives rise to a large chemical shift via the Van Vleck mechanism, as often encountered in nonmagnetic transition metal ions.

The EFG exhibits cylindrical symmetry around c, in accordance with the fact that the c axis is a C_3 symmetry element of the point group of Co I. Consistent values of the quadrupolar frequency ν_Q (proportional to the EFG) are estimated in different chain types and experimental geometries, with the notable exception of the minority chains in external longitudinal fields approaching the FI-FM transition value B_{c2}, where an EFG deviation of order −7% is found, well beyond the experimental uncertainty. We argue that a magnetoelastic coupling of the Co^{3+} ions in counteroriented minority chains might be the source of the observed EFG reduction, as already proposed for other cobalt-based compounds studied by Mössbauer spectroscopy.[31]

The internal field $B_{\rm int}$ at the nonmagnetic Co I site can be accounted for by purely dipolar interactions with the surrounding Co II spins, within an absolute accuracy of 2 mT in all of the three chain types. This result, along with the experimental value of $\hat{K}$, sets a very stringent upper limit to a transferred hyperfine field at the nucleus.

The contact hyperfine field may originate both from a tiny on-site magnetic moment on Co I, like that invoked in a neutron scattering refinement,[8] and from the coupling to nearest-neighbor Co II spins. These two contributions might partially cancel out, since either sign is possible.[24] Additional interchain contributions are negligible in view of the large chain spacing. Nevertheless, we can safely rule out an on-site term, since a residual on-site moment would require an admixture of the t_{2g} with the excited e_g orbitals, in contrast with the large crystal-field excitation energy implied by the observed moderate chemical shift value. For instance, a huge chemical shift $K \approx 5$ was reported for the resonance of ^{141}Pr in low-spin Pr^{3+}, in combination with a small fractional moment $\approx 0.01\ \mu_B$ on the Pr ion.[32] Therefore, only the transferred contribution is to be considered.

An intrachain transferred hyperfine term B_{hf} would offset the total dipolar field $B_{\rm tot}$ (Table I) by $\pm|B_{hf}|$ for the FI↑ and FM chains, and by $\mp|B_{hf}|$ for the FI↓ chains, depending on the relative signs of $B_{\rm tot}$ and B_{hf}. However, a finite B_{hf} biasing term does not improve the agreement between the calculated $B_{\rm tot} \pm B_{hf}$ and the experimentally determined internal fields. We conclude therefore that the slight discrepancy between the experimental and the calculated internal fields must be due to other sources of error, and that the contact field, if present, is much smaller than 2 mT.

A negligible hyperfine field at the Co I site is an unexpected result. Transferred hyperfine fields at nuclei of nonmagnetic ions in magnetic compounds of transition metals are typically of the order of several hundreds of millitesla or more, unless perfect cancellation occurs at a symmetric site of an AF structure, which is not the case in $Ca_3Co_2O_6$. For instance, the transferred hyperfine field at ^{139}La in the FM manganite $La_{1-x}Ca_xMnO_3$ equals 3 T, i.e., approximately 10% of the on-site hyperfine field at the Mn sites, where the magnetism resides.[33] Here, a virtually vanishing contact field at Co I indicates that there is no significant hybridization between the Co^{3+} (I) and the Co^{3+} (II) wave functions either directly or through an oxygen bridge.

The mechanisms underlying exchange and hyperfine transfer are similar, although not exactly identical.[34,35] Therefore, the lack of a detectable transferred hyperfine field strongly suggests that Co^{3+} (I) ions do not participate in the exchange interaction J_1 between two neighboring on-chain Co^{3+} (II) spins. We stress that this finding constitutes experimental evidence against the currently accepted theoretical model by Frésard *et al.*, who instead proposed an exchange path across Co I assuming a large overlap of Co^{3+} (II) with Co^{3+} (I) wave functions, yielding a direct integral $t = 1.5$ eV.[7]

B. Nature of the metamagnetic transitions: Perfect Ising behavior

At 10 K two types of field-dependent magnetic structure are detected, namely, perfect FI and FM ones, in accordance with the two plateaus in magnetization data at the same temperature. The two structures are clearly identified by distinct local fields at the Co I sites in good quantitative agreement with the dipolar fields calculated for the corresponding spin arrangements. The transition from a FI to a FM phase shows up as a sharp step in $B_{\rm int}$ at a threshold field $B_{c2} \approx 3.5$ T, revealed by an abrupt crossover of the resonance frequency vs field between two distinct $\nu_0(B_{\rm ext})$ functions (Fig. 3).

Quantitative comparison between NMR and magnetization data in longitudinal fields at 10 K (Fig. 12) provides an insight into the magnetization process. Close inspection of the magnetization curves as a function of the applied field $H \equiv B_{\rm ext}/\mu_0$ shows that the steps appear smoother in the $M(H)$ curves than in the NMR frequency data $\nu_0(B_{\rm ext})$ (Fig. 12 inset). Moreover, the plateaus in $M(H)$ are only approximately flat, with a moderate field dependence that is larger in the FI state (for instance, $\mu_0^{-1}\partial M/\partial H \approx 0.05\ \mu_B$/T for $1 < \mu_0 H < 3$ T).

In principle, incomplete saturation of $M(H)$ over the plateaus might be due to either unsaturated c axis components of individual moments in a homogeneously magnetized sample (e.g., due to spin canting), or inhomogeneous magnetization, although the former could not easily be reconciled with the known strong single-ion anisotropy of the system. NMR demonstrates experimentally that the cobalt spins are collinear and saturated even in the vicinity of the FI-FM transition. Proof is provided by the field proportionality coefficient a of Eq. (1), whose experimental values for the three chain types were found to coincide within an error $\delta a \approx 10$ kHz/T. The observed value of $\partial M/\partial H$ contributes a 15 kHz/T slope (i.e., of order δa) to $\nu_0(B_{\rm ext})$ via the demagnetization field, regardless of the mechanism responsible for it, and independent of the magnetic order in a chain. A hypothetical field-dependent canting, however, would affect the dipolar field at Co I, which is larger than the demagnetization field by an order of magnitude (Table I). Unless we assume equal canting in the FM, FI spin-up, and FI spin-down chains, which is clearly unphysical, the latter would produce differences in the a coefficients of the three lines well beyond experimental errors, and contrary to experimental evidence.

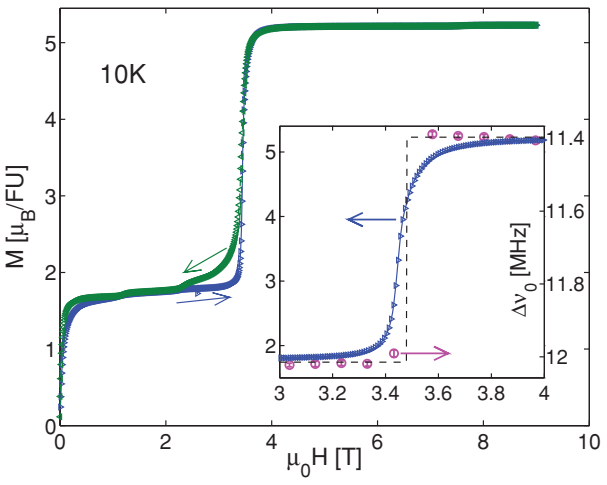

FIG. 12. (Color online) Magnetization curves at 10 K as a function of the external field H applied along c. Inset: detail of $M(H)$ across the FI-FM transition, overlaid for comparison to the frequency offsets $\Delta\nu_0 \equiv \nu_0 - aB_{\rm ext}$ of the central NMR line of either FI↑ or FM chains, where a is the best-fit parameter to Eq. (1) (whence $\Delta\nu_0 \approx b \propto B_{\rm int}$ within error).

As seen from NMR, the system apparently exhibits perfect Ising behavior. Therefore, the rounded steps in the $M(H)$ data at the field-induced metamagnetic transitions, with unsaturated magnetization over broad H intervals near them, must be due to a fraction of misoriented domains or spin chains.

C. Two distinct magnetic excitations probed by T_1^{-1} and T_2^{-1}

Further insight into the spin-reversal process close to the MPDA-FI and FI-FM transitions is provided by the large and divergent spin-spin relaxations, accompanied by much smaller and nondivergent spin-lattice relaxations. We recall that the spin-lattice relaxation rate T_1^{-1} probes transverse random magnetic fields fluctuating at the Larmor frequency ω_L, while the spin-spin rate T_2^{-1} is the sum of a term proportional to T_1^{-1} (the population term) and a secular term arising from longitudinal random fields fluctuating at virtually zero frequency.[36,37] In the presence of isotropic and fast fluctuations in the so-called narrowing limit (such that ω_L is much smaller than the roll-off frequency of the fluctuation spectrum) the two rates tend to coincide.[38] Here, the similar behavior of relaxations measured in longitudinal and oblique external fields rules out the possibility that anisotropic fluctuations, namely, entirely along the c axis and hence ineffective for spin-lattice relaxations, are the source of the huge difference in T_1 and T_2 time scales. Excess spin-spin relaxation and T_2^{-1} peaks must instead depend on fluctuations in a regime opposite to the narrowing limit, namely, with characteristic frequencies much lower than ω_L and hence contributing only to the secular term in T_2^{-1}. Such a regime, which has already been reported in the literature for other oxides,[39] is referred to hereafter as the nearly static limit.

To this end, the Kubo-Tomita theory of line shape appropriate for continuous-wave magnetic resonance[40] is modified in the context of pulsed NMR by an experimental low-frequency cutoff, namely, the reciprocal time window $\omega_c = (2\tau)^{-1}$ of a spin-echo experiment (here, τ is the time separation of the two excitation pulses). Random fields fluctuating at frequencies $\omega \ll \omega_c \approx 2 \times 10^4\ {\rm s}^{-1}$ may be viewed as static over the excitation-detection transient and contribute only to the inhomogeneous line broadening, which is refocused by the

spin-echo sequence. Conversely, fluctuations at $\omega_c < \omega \ll \omega_L$ effectively relax the spin-echo signal.

Within the nearly static limit, the decrease of T_2^{-1} with decreasing temperature (Fig. 11) then indicates the collapse of the fluctuation spectrum below the cutoff ω_c (hence, the decrease of the spectral weight above ω_c) at lower temperatures, down to a complete freezing of the spin dynamics observed at $T < 5$ K. It is worth noting that evidence for comparable time scales in the spin dynamics was also reported from χ' and χ'' ac magnetic susceptibilities in the zero-field phase, both showing a strong frequency dependence over the acoustic and subacoustic range.[41] The nearly Gaussian T_2 relaxation form is another signature of nuclear spin depolarization from quasistatic random fields.[36] In our case, random fields are clearly electronic in origin, since the calculated second moment of the nuclear dipolar fields yields a T_2^{-1} rate smaller than the observed ones by at least one order of magnitude.

The peculiar behavior of T_2^{-1} rates therefore reflects the exceedingly slow spin dynamics, as in the case of massive excitation modes involving the collective motion of several spins. In view of the strong Ising character of the system, such excitations probably consist in the coherent reversal of large portions of the spin chains or domains. The slowly fluctuating random fields responsible for spin-spin relaxation are then straightforwardly identified with the stray dipolar fields originating from such transient defects in the magnetic structure. Also the peaks in T_2^{-1} and the stretched exponent β at the metamagnetic transitions finds a natural explanation within this framework.

A peak in T_2^{-1} vs $B_{\rm ext}$ may arise in principle from either a field-dependent correlation time of fluctuations or a peak in the random field amplitude. In the nearly static fluctuation regime, however, field dependence of the correlation time would imply *faster* spin fluctuations at the peak. The latter is apparently inconsistent with the peaks in β vs $B_{\rm ext}$ reaching nearly Gaussian values of 1.5 at B_{c1} and B_{c2}, a signature of a nearly frozen spin dynamics, following the above argument. The T_2^{-1} peak must therefore originate from a corresponding increase of the quasistatic magnetic disorder, namely, a larger number of misoriented domains or chain fragments, close to the transitions. We note that the peaks of β vs $B_{\rm ext}$ coherently reflect changes in the spatial distribution of random fields on approaching the metamagnetic transitions. According to a well-known mechanism,[36,42] the transition from a quasi-Gaussian to a quasi-Lorentzian line shape may be driven by an increasing dilution of (nearly) static magnetic impurities or defects, and vice versa. Thus, the larger disorder probed by T_2^{-1} peaks consistently coincides with a larger concentration of magnetic defects indicated by $\beta > 1$, which agrees with the shortening of the magnetic coherence length observed on approaching the field-induced transitions.[43]

In contrast, spin-lattice relaxations are governed by independent excitations, whose effect on T_2 is unimportant as it is masked by the relaxation channel sketched above. The thermally activated behavior of T_1^{-1} reveals a *gap* Δ of order 100 K in their spectrum. A thorough investigation of Δ as a function of $B_{\rm ext}$ for the different chain types, and a fitting of the experimental energy gaps to a theoretical model, are the subject of a separate presentation. Here we anticipate that, according to the model, the activated spin-lattice relaxations are essentially driven by the spin flip of a single Co^{3+} moment.

D. Spin freezing: Relevance for the magnetization steps

We conclude this discussion with a comment on the low-temperature multistep behavior in $M(H)$. The magnetic structures underlying each step could not be accessed in our NMR study, due to the nonspherical shape of our sample, inducing demagnetization-dependent line broadening and offsets which prevent finer resolution of dipolar fields, as well as to exceedingly slow spin-lattice relaxations below 5 K. Nevertheless, T_2 data at 7–15 K reveal a scenario of glassy spin dynamics involving freezing of sizable magnetic aggregates and large quasistatic inhomogeneities close to the field-induced transitions. The collective arrangement of such frozen entities at lower temperature is unknown. We may argue however that it gives rise to complex field-dependent micromagnetic configurations or superstructures, resulting in a multiplicity of local minima separated by potential barriers in the free energy, becoming metastable below 2 K. If this picture holds true, however, the physical mechanism behind magnetization steps should be understood in terms of thermally assisted hopping between essentially mesoscopic metastable configurations, probably incommensurate with the crystal lattice, rather than quantum tunneling as in molecular magnets.

E. Conclusion

In conclusion, ^{59}Co NMR detects the field-induced FI and FM ordering of the Ising-type spin chains of $Ca_3Co_2O_6$ at intermediate temperature. The FI-FM and FI-MPDA metamagnetic transitions proceed through the disruption of long-range intrachain order, with no detectable deviation from spin collinearity.

NMR relaxations single out two types of magnetic excitation: a faster single-spin one, and a much slower collective reorientation of entire chain fragments which constitutes the peculiar fluctuation mode that drives the metamagnetic transitions. The latter displays glassy features (Gaussian-like spectral densities, very long correlation times, and low-temperature freezing) which are probably the clue to understanding the multistep behavior in the magnetization at low temperature.

The nonmagnetic Co^{3+} I ion apparently plays no role in the stronger intrachain exchange coupling.

ACKNOWLEDGMENTS

The authors thank S. Carretta, P. Santini, and A. Bombardi for helpful and stimulating discussions.

APPENDIX A: THE ^{59}CO RESONANCE

The resonance frequencies of ^{59}Co at the nonmagnetic site I, for an arbitrary experimental geometry, depend on the external field and sample alignment in a rather complicated way, which deserves some comment.

The field at the nucleus $\boldsymbol{B}_{\rm nuc}$ (proportional to the resonance frequency $\nu_Z = \gamma B_{\rm nuc}/2\pi$) differs from the local field $\boldsymbol{B}_{\rm loc}$ at the ion site by the chemical shift, $\boldsymbol{B}_{\rm nuc} = (1+\hat{K})\boldsymbol{B}_{\rm loc}$, where the chemical shift tensor $\hat{K}$ is usually large and anisotropic in cobalt.[30] In a magnetic material, the local field is the vector composition of the external and the internal fields, $\boldsymbol{B}_{\rm loc} = \boldsymbol{B}_{\rm ext} + \boldsymbol{B}_{\rm int}$, where the internal field $\boldsymbol{B}_{\rm int}$ originates from the electronic moments. The overall dependence of ν_Z is summarized by Eq. (2).

In the present case, the sources of $\boldsymbol{B}_{\rm int}$ are (i) the dipolar coupling with neighboring Co II spins; (ii) the net demagnetization field, namely, the difference between the demagnetization effects of the outer sample surface and a Lorentz sphere, which does not vanish due to the nonspherical shape of the sample; and (iii) possibly, a transferred hyperfine contribution, due to the polarization of wave functions. Even in a hard easy-axis magnet like the present one, the direction of magnetic moments with respect to the crystal axes, and hence of $\boldsymbol{B}_{\rm int}$, depends on $\boldsymbol{H} \approx \mu_0^{-1}\boldsymbol{B}_{\rm ext}$ via the finite transverse magnetic susceptibility χ_{ab} of the system, leading to a field-induced tilting of the Co^{3+} spins by a small but non-negligible angle $\psi \propto \chi_{ab}H_\perp$, and by $\approx -\psi/2$ for $\boldsymbol{B}_{\rm int} \approx \boldsymbol{B}_{\rm dip}$ if the dipolar contribution dominates, due to the tensorial form $B_{{\rm dip},\alpha} \propto (3k_\alpha k_\beta - \delta_{\alpha,\beta})S_\beta$ of the dipolar coupling (here $\alpha,\beta = x,y,z$, and $\boldsymbol{k}$ is the unit vector parallel to the c axis).

In a crystal, ^{59}Co ($I = 7/2$) is also coupled by its electric quadrupole moment to the local electric field gradient via a quadrupolar spin Hamiltonian of the form

$$\mathcal{H}_Q = \frac{h\nu_Q}{6}\left[3I_z^2 - I(I+1) + \frac{\eta}{2}(I_+^2 + I_-^2)\right], \qquad \text{(A1)}$$

where $I_\pm = I_x \pm iI_y$, I_x,I_y,I_z are the nuclear spin components in the crystal reference frame, and x,y,z coincide with the EFG principal axes. Here the quadrupolar frequency ν_Q is defined as a function of the nuclear quadrupole moment Q and the main component V_{zz} of the EFG tensor as $\nu_Q = 3eV_{zz}Q/[2hI(2I-1)]$, and $\eta = ||V_{yy}| - |V_{xx}||/V_{zz}$ is the EFG rhombicity factor.[36]

In the presence of a large magnetic field (either external or internal) at the nucleus, such that $\nu_Z \gg \nu_Q$, the quadrupolar interaction of Eq. (A1) behaves as a perturbation, and splits the nuclear Zeeman transitions into a multiplet of $2I$ lines. In a second-order expansion vs ν_Q/ν_Z, the frequency ν_n of the $|n-1/2\rangle \leftrightarrow |n+1/2\rangle$ Zeeman transition ($n = -I+1/2, -I+3/2, \ldots, I-1/2$) depends on $\boldsymbol{B}_{\rm nuc}$ as

$$\nu_n = \nu_Z - \frac{4\nu_Q^2}{\nu_Z}[(I+1/2)^2 - 1][2\mathcal{B}(\theta,\phi) - \mathcal{C}(\theta,\phi)] - \nu_Q\mathcal{A}(\theta,\phi)n + \frac{12\nu_Q^2}{\nu_Z}[4\mathcal{B}(\theta,\phi) - \mathcal{C}(\theta,\phi)]n^2, \qquad \text{(A2)}$$

where θ,ϕ are the polar coordinates of $\boldsymbol{B}_{\rm nuc}$ in the crystal frame, and the coefficients $\mathcal{A},\mathcal{B},\mathcal{C}$ are defined as

$$\mathcal{A}(\theta,\phi) = \tfrac{1}{2}(3\cos^2\theta - 1 + \eta\sin^2\theta\cos 2\phi),$$

$$\mathcal{B}(\theta,\phi) = \tfrac{1}{144}\sin^2\theta[\cos^2\theta(9 - 6\eta\cos 2\phi + \eta^2\cos^2 2\phi) + \eta^2\sin^2 2\phi], \qquad \text{(A3)}$$

$$\mathcal{C}(\theta,\phi) = \tfrac{1}{576}\{9\sin^4\theta + 6\eta\sin^2\theta(1+\cos^2\theta)\cos 2\phi + \eta^2[\cos^2 2\phi + 2\cos^2\theta(1+\sin^2 2\phi) + \cos^2\theta\cos^2 2\phi]\}.$$

We note that all second-order terms vanish for a cylindrical EFG ($\eta = 0$) and EFG principal axis collinear to $B_{\rm nuc}$ ($\theta = 0$).

APPENDIX B: THE SPIN-LATTICE RELAXATION FUNCTION

The approach to thermodynamic equilibrium of an ensemble of nuclear spins I is governed by a closed set of rate equations for the mth level population N_m ($m = I, \ldots, -I$). In the presence of a magnetic relaxation channel, it has the form[44]

$$\dot{N}_m = W\big[(I+m+1)(I-m)\big(N_{m+1} - N_{m+1}^{(0)}\big) + (I-m+1)(I+m)\big(N_{m-1} - N_{m-1}^{(0)}\big) - 2(I^2 - m^2 + I)\big(N_m - N_m^{(0)}\big)\big], \qquad \text{(B1)}$$

where $N_m^{(0)}$ is the population at equilibrium, and W is the transition probability $|m\rangle \leftrightarrow |m-1\rangle$ between two adjacent Zeeman levels. In the case of quadrupole-split NMR lines with the selective excitation of a single nuclear transition of order n ($n = I-1/2, \ldots, -I+1/2$), the signal intensity is proportional to the population difference $A_n \equiv N_{n+1/2} - N_{n-1/2}$ of the two levels involved, rather than the expectation value of the total spin $\langle I_z\rangle$. Solution of Eq. (B1) yields a recovery of A_n according to the superposition of $2I$ exponential components for generic n (reduced to $I+1/2$ for $n = 0$) with relative weights depending on the saturation method as well as on n.

In our experiments, the spin ensemble was prepared with a fast saturation, i.e., with a pulse train much shorter than the spin-lattice relaxation time $T_1 \equiv (2W)^{-1}$, so that populations N_m of nuclear levels $m \neq n \pm 1/2$ not involved in the transition were practically unaffected.[44,45] For the central line $n = 0$ of a $I = 7/2$ nuclear species like ^{59}Co, the recovery law following such an initial condition is then calculated as follows:

$$A_0(t) = A_0^{(0)}\left(1 - \frac{1}{84}e^{-2Wt} - \frac{3}{34}e^{-12Wt} - \frac{150}{728}e^{-30Wt} - \frac{1225}{1716}e^{-56Wt}\right). \qquad \text{(B2)}$$

*allodi@fis.unipr.it

[1] H. Fjellvåg, E. Gulbrandsen, S. Aasland, A. Olsen, and B. C. Hauback, J. Solid State Chem. **124**, 190 (1996).

[2] A. Maignan, C. Michel, A. C. Masset, C. Martin, and B. Raveau, Eur. Phys. J. B **15**, 657 (2000).

[3] T. Burnus, Z. Hu, M. W. Haverkort, J. C. Cezar, D. Flahaut, V. Hardy, A. Maignan, N. B. Brookes, A. Tanaka, H. H. Hsieh,

H.-J. Lin, C. T. Chen, and L. H. Tjeng, Phys. Rev. B **74**, 245111 (2006).
[4]E. V. Sampathkumaran, N. Fujiwara, S. Rayaprol, P. K. Madhu, and Y. Uwatoko, Phys. Rev. B **70**, 014437 (2004).
[5]R. Vidya, P. Ravindran, H. Fjellvåg, A. Kjekshus, and O. Eriksson, Phys. Rev. Lett. **91**, 186404 (2003).
[6]Hua Wu, M. W. Haverkort, Z. Hu, D. I. Khomskii, and L. H. Tjeng, Phys. Rev. Lett. **95**, 186401 (2005).
[7]R. Frésard, C. Laschinger, T. Kopp, and V. Eyert, Phys. Rev. B **69**, 140405(R) (2004).
[8]S. Aasland, H. Fjellvåg, and B. Hauback, Solid State Commun. **101**, 187 (1997).
[9]M. Mekata, J. Phys. Soc. Jpn. **42**, 76 (1977).
[10]K. Wada and T. Ishikawa, J. Phys. Soc. Jpn. **52**, 1774 (1983).
[11]H. Kageyama, K. Yoshimura, K. Kosuge, H. Mitamura, and T. Goto, J. Phys. Soc. Jpn. **66**, 1607 (1997).
[12]H. Kageyama, K. Yoshimura, K. Kosuge, X. Xu, and S. Kawano, J. Phys. Soc. Jpn. **67**, 357 (1998).
[13]O. A. Petrenko, J. Wooldridge, M. R. Lees, P. Manuel, and V. Hardy, Eur. Phys. J. B **47**, 79 (2005).
[14]S. Agrestini, C. Mazzoli, A. Bombardi, and M. R. Lees, Phys. Rev. B **77**, 140403(R) (2008).
[15]S. Agrestini, L. C. Chapon, A. Daoud-Aladine, J. Schefer, A. Gukasov, C. Mazzoli, M. R. Lees, and O. A. Petrenko, Phys. Rev. Lett. **101**, 097207 (2008).
[16]A. Maignan, V. Hardy, S. Hebert, M. Drillon, M. R. Lees, O. Petrenko, D. Mc K. Paul, and D. Khomskii, J. Mater. Chem. **14**, 1231 (2004).
[17]V. Hardy, M. R. Lees, O. A. Petrenko, D. McK. Paul, D. Flahaut, S. Hébert, and A. Maignan, Phys. Rev. B **70**, 064424 (2004).
[18]Y. B. Kudasov, Phys. Rev. Lett. **96**, 027212 (2006).
[19]Y. Shimizu, M. Horibe, H. Nanba, T. Takami, and M. Itoh, Phys. Rev. B **82**, 094430 (2010).
[20]V. Hardy, S. Lambert, M. R. Lees, and D. McK. Paul, Phys. Rev. B **68**, 014424 (2003).
[21]G. Allodi, A. Banderini, R. De Renzi, and C. Vignali, Rev. Sci. Instrum. **76**, 083911 (2005).
[22]C. S. Lue, Y. T. Lin, and C. N. Kuo, Phys. Rev. B **75**, 075113 (2007).
[23]M. Pieper, H. Niki, U. Seto, E. Gratz, K. Hense, N. Stuesser, V. Paul-Boncour, A. S. Markosyan, and A. Hoser, J. Magn. Magn. Mater. **272–276**, E389 (2004).
[24]H. Yoshie and Y. Nakamura, J. Phys. Soc. Jpn. **57**, 3157 (1988).
[25]Hereafter we denote as B_n the position of the nth quadrupole satellite in a field-sweep spectrum at a fixed frequency ν_L, implicitly defined by the equation $\nu_n(B_n) - \nu_L = 0$, where $\nu_n(B_{\rm ext})$ is the resonance frequency of the nth satellite in an external field $B_{\rm ext}$.
[26]We remark that powder average of line patterns like the present ones would actually lead to NMR spectra with "more than one [signal] with different centers of gravity," as pointed out in Ref. 4. However, the bimodal spectra there simply reflect the presence of a FI volume fraction in the sample, whereby majority and minority chains give rise to positive and negative internal fields, respectively.
[27]In principle, the azimuthal dependence of the central resonance [Fig. 8(b)] might be also affected by a a noncylindrical chemical shift tensor ($K_a \neq K_b$). However, our finding of $K_\perp$ independent of ϕ within experimental error ($\Delta K_\perp = 2\times10^{-4}$) rules out a significant contribution of the chemical shift, whose residual rhombicity would anyway produce the same unobserved angular periodicity by π as the EFG. For both quantities, a cylindrical tensor is furthermore imposed by the $R\bar{3}c$ space group of the system, well established by x-ray and neutron diffraction (Ref. 1).
[28]L. D. Landau and E. M. Lifshitz, *Electrodynamics of Continuous Media* (Pergamon, Oxford, 1984).
[29]The ^{59}Co gyromagnetic ratio is determined as $^{59}\gamma/2\pi = 10.10$ MHz/T from a $K_3Co(CN)_6$ aqueous solution reference; see, e.g., Ref. 22. In the literature there is however large dispersion in the reported values for $^{59}\gamma$, due to the large chemical shifts of ^{59}Co and the uncertainty on a zero-shift reference (Ref. 30).
[30]J. C. C. Chan and S. C. F. Au-Yeung, Annu. Rep. NMR Spectrosc. **41**, 1 (2000).
[31]D. C. Price, B. D. Howes, and M. C. K. Wiltshire, J. Phys. C: Solid State Phys. **17**, 3645 (1984).
[32]K. Nehrke and M. W. Pieper, Phys. Rev. Lett. **76**, 1936 (1996).
[33]G. Allodi, R. De Renzi, F. Licci, and M. W. Pieper, Phys. Rev. Lett. **81**, 4736 (1998).
[34]P. W. Anderson, in *Magnetism I*, edited by G. T. Rado and H. Suhl (Academic Press, New York, 1963).
[35]A. J. Freeman and R. E. Watson, in *Magnetism IIA*, edited by G. T. Rado and H. Suhl (Academic Press, New York, 1965).
[36]A. Abragam, *The Principles of Nuclear Magnetism* (Clarendon Press, Oxford, 1961).
[37]C. P. Slichter, *Principles of Magnetic Resonance* (Springer, New York, 1990).
[38]In the present case of EFG-perturbed NMR with resolved quadrupole satellites, rate equations predict an asymptotic constant ratio T_2^{-1}/T_1^{-1} larger than unity, equal to 16 for the central line of ^{59}Co ($I = 7/2$). See, e.g., R. R. Ernst, G. Bodenhausen, and A. Wokaun, *Principles of Nuclear Magnetic Resonance in One and Two Dimensions* (Oxford University Press, Oxford, 1987), p. 55.
[39]G. Allodi, M. Cestelli Guidi, R. De Renzi, A. Caneiro, and L. Pinsard, Phys. Rev. Lett. **87**, 127206 (2001).
[40]R. Kubo and K. Tomita, J. Phys. Soc. Jpn. **9**, 888 (1954).
[41]V. Hardy, D. Flahaut, M. R. Lees, and O. A. Petrenko, Phys. Rev. B **70**, 214439 (2004).
[42]R. E. Walstedt and L. P. Walker, Phys. Rev. B **9**, 4857 (1974).
[43]C. Mazzoli, A. Bombardi, S. Agrestini, and M. R. Lees, Physica B **404**, 3042 (2009).
[44]A. Narath, Phys. Rev. **162**, 320 (1967).
[45]T. Rega, J. Phys. Condens. Matter **3**, 1871 (1991).